energies

MDPI

Article

Fired Heaters Optimization by Estimating Real-Time Combustion Products Using Numerical Methods

Ricardo Sánchez [1], Argemiro Palencia-Díaz [1,*], Jonathan Fábregas-Villegas [1,2] and Wilmer Velilla-Díaz [3,*]

[1] Department of Mechanical Engineering, Universidad Tecnológica de Bolivar, Cartagena 130001, Colombia; sanchezr@utb.edu.co (R.S.); jfabregas@utb.edu.co (J.F.-V.)
[2] Industrial Engineering Program, Universidad Sergio Arboleda, Barranquilla 081007, Colombia
[3] Department of Mechanical Engineering, Universidad de La Serena, La Serena 1720170, Chile
* Correspondence: argpalencia@utb.edu.co (A.P.-D.); wilmer.velilla@userena.cl (W.V.-D.)

Abstract: Fired heaters upstream of distillation towers, despite their optimal thermal efficiency, often suffer from performance decline due to fluctuations in fuel composition and unpredictable operational parameters. These heaters have high energy consumption, as fuel properties vary depending on the source of the crude oil. This study aims to optimize the combustion process of a three-gas mixture, mainly refinery gas, by incorporating more stable fuels such as natural gas and liquefied petroleum gas (LPG) to improve energy efficiency and reduce LPG consumption. Using real-time gas chromatography-mass spectrometry (GC-MS) data, we accurately calculate the mass fractions of individual compounds, allowing for more precise burner flow rate determinations. Thermochemical data are used to calculate equilibrium constants as a function of temperature, with the least squares method, while the Newton–Raphson method solves the resulting nonlinear equations. Four key variables (X_4, X_6, X_8, and X_{11}), representing H_2, CO, O_2, and N_2, respectively, are defined, and a Jacobian matrix is constructed to ensure convergence within a tolerance of 1×10^{-6} over a maximum of 200 iterations, implemented via Python 3.10.4 and the scipy.optimize library. The optimization resulted in a reduction in LPG consumption by over 50%. By tailoring the fuel supply to the specific thermal needs of each processing unit, we achieved substantial energy savings. For instance, furnaces in the hydrocracking unit, which handle cleaner subproducts and benefit from hydrogen's adiabatic reactions, require much less energy than those in the primary distillation unit, where high-impurity crude oil is processed.

Keywords: optimizing combustion; adiabatic flame; Newton–Raphson; fired heaters; refinery gas

check for updates

Citation: Sánchez, R.; Palencia-Díaz, A.; Fábregas-Villegas, J.; Velilla-Díaz, W. Fired Heaters Optimization by Estimating Real-Time Combustion Products Using Numerical Methods. *Energies* **2024**, *17*, 6190. https://doi.org/10.3390/en17236190

Academic Editor: Qingsong Wang

Received: 28 August 2024
Revised: 20 September 2024
Accepted: 29 September 2024
Published: 9 December 2024

1. Introduction

In a wide range of refinery configurations, heaters are strategically positioned upstream of the crude distillation tower to ensure that the incoming crude oil is heated to a specific, required temperature. This temperature regulation is imperative for optimal operation. In instances where the crude oil does not attain this essential temperature, it becomes necessary to either increase the combustion of fuel gas or adjust the calorific value of the gas mixture. This adjustment is essential to achieve the desired process temperature, underscoring the importance of thermal management and energy efficiency in refinery operations. Fired heaters represent the primary energy consumers in both the refining and petrochemical sectors, with approximately 55% of total energy consumption being attributed to their function as heat exchangers [1]. Although most were designed for thermal efficiencies of up to 80%, current operating efficiencies often fall short of expectations [2]. This is thought to result from the inconsistent operation of the furnaces in line with their design conditions.

Hydrocarbons have played a crucial role in the global economy for centuries, acting as key drivers of industrial development [3–6]. Hydrocarbons in the gaseous state serve as a common fuel burned in this equipment [7,8]. However, exclusive reliance on one type of gas is not feasible due to source limitations. This leads to increased costs and insufficient combustion efficiency. Currently, a mixture of natural gas (NG) and refinery gas (RG) is used as the primary fuel source in industrial applications [9]. RG is usually recovered from various processes, including cracking, desulphurization, and catalytic reforming units [10]. Liquefied petroleum gas (LPG), a by-product of crude oil refining, is occasionally used as a third gas due to its high propane and butane content, which increases the calorific value of the mixture. This is particularly useful when the mixture of NG and RG has a significantly low calorific value or when considering the fluctuating costs of these fuels in the market [11]. These procedures generate a diverse matrix of fuel blends, resulting in a wide range of compositions suitable for combustion processes [12]. Highlighting that NG and LPG are relatively more environmentally friendly, their combustion produces lower pollutant emissions into the atmosphere [13].

The optimization of thermal efficiency in fired heaters can be achieved through different strategies [14–16]. Thorat and Garg, both emphasize the importance of optimal design and application of heat tracing and management systems, which can significantly reduce energy consumption [2,17]. Masoumi further underscores the potential for improvement in refinery furnaces' efficiency through mathematical modeling, particularly by considering ambient and operational conditions [18]. These studies collectively highlight the need for a holistic approach to addressing the challenges of energy usage in petrochemical refineries. It has also been emphasized that net-zero global carbon dioxide CO_2 emissions need to be reached to achieve this goal by 2050 [19]. Thus, reducing greenhouse gas emissions, especially CO_2, is one of the main global challenges to achieving a more sustainable future. Combustion furnaces within oil refineries generally account for over 65% of CO_2 emissions [20]. Single-burner research furnaces have undergone testing, revealing staged combustion air injection and flue gas recirculation as the most promising combustion modifications to decrease NO emissions from the gas-fired process heater. The modifications have a potential for up to a 67% reduction [21].

Research also highlights the significance of fuel composition, particularly hydrogen enrichment, in enhancing combustion efficiency. Additionally, experts are developing simulation methods for optimizing gaseous fuel mixtures [22–26]. Saifullin's specialized techniques have significantly improved combustion efficiency in thermal power plants that use variable fuel compositions [27]. Some researchers have studied real-time optimization [28]. However, there is still a gap in the real-time optimization of fuel mixtures, particularly for RG, when responding to their changing compositions. Gas chromatography-mass spectrometry (GC-MS) data play a vital role in comprehending RG behavior. In an industrial context, it is important to maintain a constant calorific value, which is critical for cost management as outlined by Cote [29]. The imperative to maintain a consistent calorific value drives many end-users to monitor and regulate their flue gas quality [30]. Chomiak observes that the utilization of gas with higher calorific value can minimize expenses linked to fuel consumption, thereby affecting the profitability per cubic meter of refined crude oil [31,32].

This study aims to bridge the knowledge gap by developing a method to dynamically optimize the combustion of a three-gas mixture. We utilize GC-MS data to analyze RG in real time, determining the mass fraction of individual compounds. These data enable the selection of optimal flow rate combinations for burners, ensuring efficient combustion. Equilibrium constants are also calculated as a function of temperature by applying the Newton–Raphson method in Python to solve the resulting nonlinear equations [33]. The research extends beyond theoretical analysis, incorporating simulations validated with in situ chromatography data. The novel aspect of this research lies in its real-time approach to optimizing fuel mixtures, examining the inherent variability of RG. This approach is expected to contribute to a significant reduction in LPG consumption, thereby offering substantial economic benefits to oil companies. Additionally, the study contributes to the broader goal of enhancing the overall efficiency and performance of furnaces in the petrochemical industry.

The paper is structured as follows: Section 2 details the setup of chemical reactions involved in combustion and the dynamic model of the gas mixture. Section 2.2 discusses the reduction in equations from twelve variables to four, which is essential for accurately computing combustion product mass fractions. Section 3 presents the method's numerical performance, supported by simulations and real-time chromatography data. Finally, Section 4 offers conclusions, highlighting the study's contributions to efficient energy management in fired heaters.

2. Methodology and Simulation Model

2.1. Composition and Properties of Gas Mixture

This research addresses the combustion of a three-gas mixture, with a particular focus on how the varying composition of RG (shown as a dashed yellow line in Figure 1) affects the process, alongside NG and a standard gas mixture (depicted by the green and red lines, respectively).

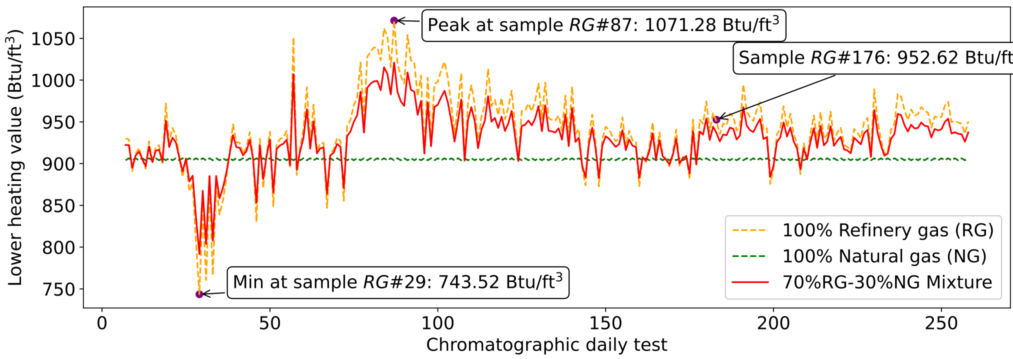

Figure 1. Daily Gas Sample Data Recorded and Analyses.

One of the key properties of gases is their ability to mix uniformly with each other, resulting in a solution where each gas component can be analyzed independently while maintaining the same temperature and volume within the mixture [34]. Understanding gas mixtures becomes more straightforward with knowledge of their composition, which we investigated through a review of statistical reports from approximately 250 chromatography analyses of RG streams collected every 24 h. Table 1 outlines the composition of three specific refinery gases at 29, 87 and 176 days, thus: $\boldsymbol{RG_{29}}$, $\boldsymbol{RG_{87}}$, and $\boldsymbol{RG_{176}}$ (See Figure 1), which represent a range of refinery gas compositions with varying calorific values and sulfur content. These gases were selected due to their distinct low heating value (LHV), thus, the minimum LHV $\boldsymbol{RG_{29}}$, the maximum LHV $\boldsymbol{RG_{87}}$, and the last one with a typical sulfur content in $\boldsymbol{RG_{176}}$. In addition, the composition of natural gas (NG) is predominantly methane (98%), while LPG is primarily composed of butane (98%), making both ideal for numerical modeling purposes due to their stable and predictable compositions. Our code is developed to flexibly process chromatographic data for these gases across various process parameters.

For the calculation of the thermodynamic properties of the air–fuel mixture, the engineering equations solver (EES) software (https://fchartsoftware.com/ees/, accessed on 19 September 2024) was used, where NASA's ideal gas data were taken. These data consist of specific heat, specific enthalpy and density, among others, at standard pressure as a function of temperature. Another advantage is the ease of numerically solving thousands of coupled non-linear algebraic and differential equations.

But first, as we observe in Table 1, none of the refinery gas samples yield the sum of the volumetric composition equal to 1 as the other two gases, so it must be readjusted to give exactly 1. Implementing them guarantees the precision of the solution for a great variety of systems, in a wide range of conditions with a high degree of efficiency and reliability.

Table 1. Selecting gases for the numerical model (MF = Mole Fraction).

Fuels Comp.	RG_{29} MF	RG_{87} MF	RG_{176} MF	NG MF	LPG MF
H_2	0.16983526	0.28839122	0.15382659	0.0	0.0
CO_2	0.00355668	0.0018357	0.00180876	0.0	0.0
CH_4	0.50036226	0.49431918	0.63173331	0.9831	0.0
C_2H_6	0.1371265	0.04462025	0.11880152	0.00258124	0.9838
C_2H_4	0.05565108	0.03992771	0.04821289	0.0	0.0
C_3H_8	0.0549727	0.0147482	0.00479593	0.002	0.0054
propylene	0.02094179	0.00305931	0.00649243	0.0	0.0098
H_2S	0.0	0.0	0.00327537	0.0	0.001
C_2H_2	7.54×10^{-6}	0.0	6.62×10^{-6}	0.0	0.0
isobutane	0.00558021	0.004937739	0.00230704	0.0	0.0
propadiene	0.0	0.0	0.0	0.0	0.0
n-butane	0.00679208	0.00343208	0.00306676	0.0	0.0
O_2	0.0004077	0.0153073	0.00022166	0.001	0.0
trans-2-butene	0.0032849	0.0023618	0.0013005	0.0	0.0
N_2	0.0212296	0.080129	0.0109625	0.011	0.0
1-butene	0.0032146	0.00032	0.0010858	0.0	0.0
isobutene	0.0042796	0.0008848	0.0009842	0.0	0.0
2-butene	0.0022651	0.0015048	1.32×10^{-5}	0.0	0.0
isopentene	0.0020144	0.000221	0.0022329	0.0002048	0.0
n-pentane	0.00162679	5.559×10^{-5}	0.0021111	6.879×10^{-5}	0.0
1,3-butadiene	0.0001166	0.0	4.06×10^{-5}	0.0	0.0
CO	0.00653259	0.0039111	0.0067198	0.0	0.0
Hexans+	0.0002015	3.27×10^{-5}	0.0	3.03×10^{-5}	0.0
$\sum X_i \equiv 1$	0.9999994	0.99999949	0.99999948	0.99998514	1.0

2.2. Chemical Reactions in the Combustion Process

Considering a fuel with a composition of C, H, O, N and S, mixed with air at an equivalence ratio denoted as ϕ, and examining its reaction in the framework of equilibrium thermodynamics applied to the system, we observe the formation of products at a temperature set as T and a pressure set as P [35]. Under conditions where high temperatures induce dissociation, up to 12 combustion products can be generated [36].

The entire representation of the chemical reaction can be formulated as follows,

$$\begin{aligned} & X_{14}[C_{n1} + H_{m1} + O_{l1} + N_{k1} + S_{j1}] + X_{15}[C_{n2} + H_{m2} + O_{l2} + N_{k2} + S_{j2}] \\ & \quad + X_{16}[C_{n3} + H_{m3} + O_{l3} + N_{k3} + S_{j3}] + \left[\frac{(n+j+\frac{m}{4}-\frac{l}{2})}{\phi}\right](O_2 + 3.76N_2) \Rightarrow \\ & X_1H + X_2O + X_3N + X_4H_2 + X_5OH + X_6CO + X_7NO \\ & \quad + X_8O_2 + X_9H_2O + X_{10}CO_2 + X_{11}N_2 + X_{12}SO_2 \end{aligned} \tag{1}$$

where j, k, l, m and n are the quantities of S, N, O, H and C, respectively, for the gases $1 = X_{14}, 2 = X_{15}$, and $3 = X_{16}$. In this context, X_{14}, X_{15}, and X_{16} represent the quantities of refinery gas, natural gas, and liquefied petroleum gas, respectively, constituting the entirety of the fuel blend. The values ranging from X_1 to X_{12} are the mole fraction of the combustion products. For the sake of simplicity, we treat air as a mixture consisting solely of O_2 and $3.76N_2$, disregarding other components. The quantity of air utilized in the combustion process depends directly on the fuel, and the concentration of air is defined by $[(n + j + m/4 - l/2)/\phi](O_2 + 3.76N_2)$, where, $j = X_{14}j1 + X_{15}j2 + X_{16}j3$; $k = X_{14}k1 + X_{15}k2 + X_{16}k3$; $l = X_{14}l1 + X_{15}l2 + X_{16}l3$; $m = X_{14}m1 + X_{15}m2 + X_{16}m3$ and $n = X_{14}n1 + X_{15}n2 + X_{16}n3$.

The equivalence ratio between air and fuel, denoted as ϕ, is defined as follows:

$$\phi = \begin{cases} > 1, & \text{for fuel-rich mixtures,} \\ = 1, & \text{for a stoichiometric mixture,} \\ < 1, & \text{for mixtures that are fuel-lean.} \end{cases}$$

The excess air coefficient is another commonly used parameter for characterizing the stoichiometry of the fuel-air mixture, and it is related to the equivalence ratio as $(1-\phi)/\phi \times 100\%$. By simplifying the expression, we used X_{13} as the sum of all the reactants, $r_0 = (n + j + m/4 - l/2)/\phi$, $r_1 = l/2 + r_0$, and $r_2 = k/2 + 3.76r_0$. Therefore, we arrive at the following equation:

$$\begin{aligned} &X_{13}({}_nC +_m H +_{r_1} O +_{r_2} N +_j S) \Rightarrow \\ &X_1H + X_2O + X_3N + X_4H_2 + X_5OH + X_6CO + X_7NO + X_8O_2 + X_9H_2O + X_{10}CO_2 + X_{11}N_2 + X_{12}SO_2 \end{aligned} \tag{2}$$

This represents the atom balance for the general equation.

$$C : nX_{13} = X_6 + X_{10} \tag{3}$$

$$H : mX_{13} = X_1 + 2X_4 + X_5 + 2X_9 \tag{4}$$

$$O : 2r_1X_{13} = X_2 + X_5 + X_6 + X_7 + 2X_8 + X_9 + 2X_{10} + 2X_{12} \tag{5}$$

$$N : 2r_2X_{13} = X_3 + X_7 + 2X_{11} \tag{6}$$

$$S : jX_{13} = X_{12} \tag{7}$$

In addition, a condition is introduced in this system which requires that the total sum of the mole fractions of all products be equal to one mole. Therefore, this implies:

$$\sum_{i=1}^{12} X_i = 1 \tag{8}$$

To solve the system of six equations (from Equations (3)–(8)) with 13 unknowns, an additional set of seven equations is required (from Equations (10)–(16)). These equations are sourced from the equilibrium reactions.

Gas Equilibrium Constants

The equilibrium constant (K_p) is determined by the ratio of the molar concentrations (mol/L) of reactants and products in a chemical reaction. Its value is temperature-dependent and must always be specified [37]. We begin by examining the general chemical reaction to determine the equilibrium constants. The equation that defines equilibrium constants as a function of partial pressures for a given combustion reaction is as follows:

$$K_p = \frac{\Pi_i (P_i/P)^{\mu_i}}{\Pi_j (P_j/P)^{\mu_j}} \tag{9}$$

where the partial pressures of flue gases are represented by $P_i/P = X_i$ and the respective stoichiometric coefficients by μ_i. The seven missing equations to solve the system correspond to the seven chemical reactions associated with natural gas, according to Olikara as follows [34].

$$\frac{1}{2}H_2 \Rightarrow H \qquad K_{p1} = \frac{X_1}{X_4^{\frac{1}{2}}} \tag{10}$$

$$\frac{1}{2}O_2 \Rightarrow O \qquad K_{p2} = \frac{X_2}{X_8^{\frac{1}{2}}} \tag{11}$$

$$\frac{1}{2}N_2 \Rightarrow N \qquad K_{p3} = \frac{X_3}{X_{11}^{\frac{1}{2}}} \tag{12}$$

$$\frac{1}{2}O_2 + \frac{1}{2}H_2 \Rightarrow OH \qquad K_{p5} = \frac{X_5}{X_4^{1/2}X_8^{1/2}} \tag{13}$$

$$\frac{1}{2}O_2 + \frac{1}{2}N_2 \Rightarrow NO \qquad K_{p7} = \frac{X_7}{X_8^{1/2}X_{11}^{1/2}} \tag{14}$$

$$H_2 + \frac{1}{2}O_2 \Rightarrow H_2O \qquad K_{p9} = \frac{X_9}{X_4 X_8^{1/2}} \tag{15}$$

$$CO + \frac{1}{2}O_2 \Rightarrow CO_2 \qquad K_{p10} = \frac{X_{10}}{X_6 X_8^{1/2}} \tag{16}$$

Applying Equation (9), the equilibrium constants data were taken from JANAF Thermochemical Tables [34], where $\log_{10} K_p$ formation for all species are tabulated as functions of the absolute temperature (K). Theoretical investigations [38] propose a functional relationship of this nature to compute the K_p as follows:

$$\log K_p = A \ln T_A + \frac{B}{T_A} + C + DT_A + ET_A^2 \tag{17}$$

where a transformed temperature T_A defined as 0.005 $T/9$ (T is in °R) was used for fitting. The constants A, B, C, D and E are listed in Table 2. This model was used to fit tabulated data through a least squares fitting method. To strike a balance between precision and temperature range, we chose the 1500 to 3000 K (2700 to 5400 °R) range for studying combustion purposes [39]. The adiabatic flame temperature, representing the maximum possible temperature without heat exchange with the surroundings, is crucial for optimizing combustion. Understanding this temperature helps minimize harmful emissions, maximize efficiency, and determine the ideal air–fuel mixture and fuel blends. Figure 2 illustrates a case of combustion wherein the adiabatic flame would attain a peak temperature of approximately 2000 K (3600 °R). Consequently, K_p values are computed simultaneously for each of the reactions.

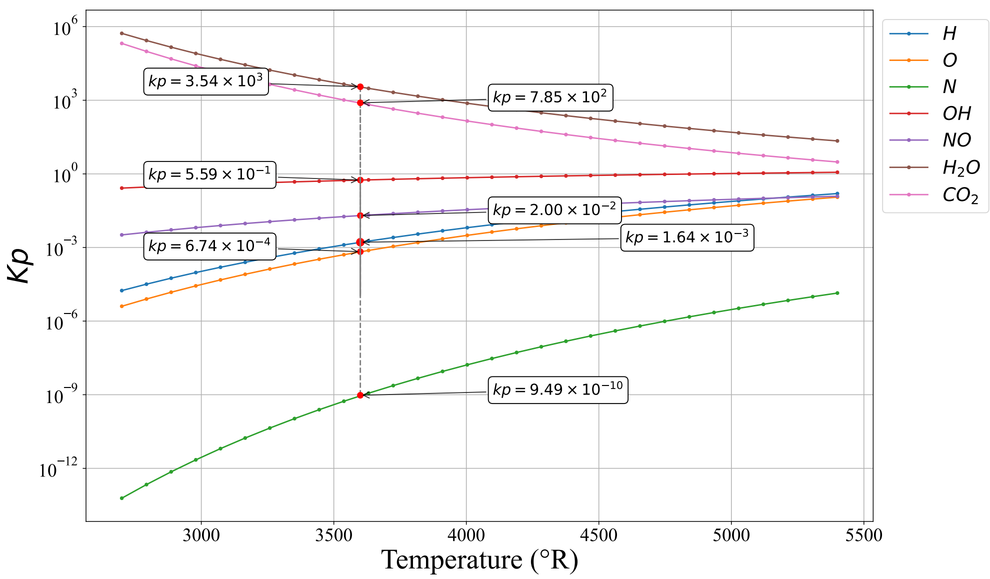

Figure 2. Equilibrium Constants K_p at 3600 °R.

Table 2. Constant coefficients of Reactions.

Equation	*A*	*B*	*C*	*D*	*E*
(10)	0.432168	-0.112464×10^{2}	0.267269×10^{1}	-0.7457×10^{-1}	0.242484×10^{-2}
(11)	0.310805	-0.129540×10^{2}	0.321779×10^{1}	-0.7383×10^{-1}	0.344645×10^{-2}
(12)	0.389716	-0.245828×10^{2}	0.314505×10^{1}	-0.9637×10^{-1}	0.585643×10^{-2}
(13)	−0.141784	-0.213308×10^{1}	0.853461	0.355015×10^{-1}	-0.3102×10^{-2}
(14)	0.150879×10^{-1}	-0.470959×10^{1}	0.646096	0.272805×10^{-2}	-0.1544×10^{-2}
(15)	−0.752364	0.124210×10^{2}	-0.260286×10^{1}	0.259556	-0.1626×10^{-1}
(16)	-0.4153×10^{-2}	0.148627×10^{2}	-0.475746×10^{1}	0.124699	-0.9002×10^{-2}

The log K_p values computed from the equations were compared with the original data, showing deviations of less than 0.0009, these deviations are considered negligible. In the process of data collection, we observe the following expressions, where the values of the variables are influenced by specific constants: $X_1 = K_{p1}\sqrt{X_4}$, $X_2 = K_{p2}\sqrt{X_8}$, $X_3 = K_{p3}\sqrt{X_{11}}$, $X_5 = K_{p5}\sqrt{X_4X_8}$, $X_7 = K_{p7}\sqrt{X_8X_{11}}$, $X_9 = K_{p9}X_4\sqrt{X_8}$, $X_{10} = K_{p10}X_6\sqrt{X_8}$. When expressing the molar fractions using the equilibrium constants in Equations (3)–(7), we decrease the number of constraints, resulting in a fresh system of four nonlinear equations with four unknowns. This means that every fraction is depending only on X_4, X_6, X_8, and X_{11} (H_2, CO, O_2, and N_2) exclusively as follows:

$$K_{p1}\sqrt{X_4} + 2X_4 + K_{p5}\sqrt{X_4X_8} + 2K_{p9}X_4\sqrt{X_8} - d_1(X_6 + K_{p10}X_6\sqrt{X_8}) = 0 \tag{18}$$

$$K_{p2}\sqrt{X_8} + K_{p5}\sqrt{X_4X_8} + X_6 + K_{p7}\sqrt{X_8X_{11}} + 2X_8 + K_{p9}X_4\sqrt{X_8} + AA = 0 \tag{19}$$

where $AA = 2K_{p10}X_6\sqrt{X_8} - d_2(X_6 + K_{p10}X_6\sqrt{X_8})$

$$K_{p3}\sqrt{X_{11}} + K_{p7}\sqrt{X_8X_{11}} + 2X_{11} - d_3(X_6 + K_{p10}X_6\sqrt{X_8}) = 0 \tag{20}$$

$$K_{p1}\sqrt{X_4} + K_{p2}\sqrt{X_8} + K_{p3}\sqrt{X_{11}} + X_4 + K_{p5}\sqrt{X_4X_8} + X_6 + K_{p7}\sqrt{X_8X_{11}} + BB = 0 \tag{21}$$

where $BB = X_8 + K_{p9}X_4\sqrt{X_8} + K_{p10}X_6\sqrt{X_8} + X_{11} + d_4(X_6 + K_{p10}X_6\sqrt{X_8}) - 1$, where $d_1 = m/n$, $d_2 = 2r_0/n$, $d_3 = 2r_1/n$, and $d_4 = r_2/n$. This set of four interrelated nonlinear equations can be expressed as a function involving four variables: $f_i(X_4, X_6, X_8, X_{11})$, here $i = 1, 2, 3, 4$.

To linearize Equations (18)–(21), a Taylor series expansion is applied, yielding the following generalized expression.

$$f_i + \frac{\partial f_i}{\partial X_4}\Delta X_4 + \frac{\partial f_i}{\partial X_6}\Delta X_6 + \frac{\partial f_i}{\partial X_8}\Delta X_8 + \frac{\partial f_i}{\partial X_{11}}\Delta X_{11} = 0 \tag{22}$$

2.3. Numerical Modeling of the Combustion Process

Using real-time gas chromatography–mass spectrometry (GC-MS) data, we accurately calculate the mole fractions of individual compounds, allowing for more precise burner flow rate determinations. Thermochemical data are used to calculate equilibrium constants as a function of temperature, with the least squares method, while the Newton–Raphson method solves the resulting nonlinear equations. The system of four nonlinear equations is solved using a 4×4 Jacobian matrix of first-order derivatives to ensure convergence within a tolerance of 1×10^{-6} over a maximum of 200 iterations (See Equation (23)). The optimization method is implemented in Python using the scipy.optimize library and the newton() function.

$$\begin{bmatrix} \frac{\partial f_1}{\partial X_4} & \frac{\partial f_1}{\partial X_6} & \frac{\partial f_1}{\partial X_8} & \frac{\partial f_1}{\partial X_{11}} \\ \frac{\partial f_2}{\partial X_4} & \frac{\partial f_2}{\partial X_6} & \frac{\partial f_2}{\partial X_8} & \frac{\partial f_2}{\partial X_{11}} \\ \frac{\partial f_3}{\partial X_4} & \frac{\partial f_3}{\partial X_6} & \frac{\partial f_3}{\partial X_8} & \frac{\partial f_3}{\partial X_{11}} \\ \frac{\partial f_4}{\partial X_4} & \frac{\partial f_4}{\partial X_6} & \frac{\partial f_4}{\partial X_8} & \frac{\partial f_4}{\partial X_{11}} \end{bmatrix} \begin{bmatrix} \Delta X_4 \\ \Delta X_6 \\ \Delta X_8 \\ \Delta X_{11} \end{bmatrix} = \begin{bmatrix} -f_1 \\ -f_2 \\ -f_3 \\ -f_4 \end{bmatrix} \tag{23}$$

The matrix equation in the expanded form is as follows:

$$\begin{bmatrix} \frac{k_{p1}}{2\sqrt{X_4}} + \frac{k_{p5}\sqrt{X_8}}{2\sqrt{X_4}} + 2k_{p9}\sqrt{X_8} + 2 & -d_1 k_{p10}\sqrt{X_8} - d_1 & -\frac{d_1 k_{p10} X_6}{2\sqrt{X_8}} + \frac{k_{p5}\sqrt{X_4}}{2\sqrt{X_8}} + \frac{k_{p9} X_4}{\sqrt{X_8}} & 0 \\ \frac{k_{p5}\sqrt{X_8}}{2\sqrt{X_4}} + k_{p9}\sqrt{X_8} & d_5 + d_6 k_{p10}\sqrt{X_8} & \frac{d_6 k_{p10} X_6}{2\sqrt{X_8}} + \frac{k_{p2}}{2\sqrt{X_8}} + \frac{k_{p5}\sqrt{X_4}}{2\sqrt{X_8}} + \frac{k_{p7}\sqrt{X_{11}}}{2\sqrt{X_8}} + \frac{k_{p9} X_4}{2\sqrt{X_8}} + 2 & \frac{k_{p7}\sqrt{X_8}}{2\sqrt{X_{11}}} \\ 0 & -d_3 k_{p10}\sqrt{X_8} - d_3 & -\frac{d_3 k_{p10} X_6}{2\sqrt{X_8}} + \frac{k_{p7}\sqrt{X_{11}}}{2\sqrt{X_8}} & \frac{k_{p3}}{2\sqrt{X_{11}}} + \frac{k_{p7}\sqrt{X_8}}{2\sqrt{X_{11}}} + 2 \\ \frac{k_{p1}}{2\sqrt{X_4}} + \frac{k_{p5}\sqrt{X_8}}{2\sqrt{X_4}} + k_{p9}\sqrt{X_8} + 1 & d_7 k_{p10}\sqrt{X_8} + d_7 & \frac{d_7 k_{p10} X_6}{2\sqrt{X_8}} + \frac{k_{p2}}{2\sqrt{X_8}} + \frac{k_{p5}\sqrt{X_4}}{2\sqrt{X_8}} + \frac{k_{p7}\sqrt{X_{11}}}{2\sqrt{X_8}} + \frac{k_{p9} X_4}{2\sqrt{X_8}} + 1 & \frac{k_{p3}}{2\sqrt{X_{11}}} + \frac{k_{p7}\sqrt{X_8}}{2\sqrt{X_{11}}} \end{bmatrix}$$

$$\begin{bmatrix} \Delta X_4 \\ \Delta X_6 \\ \Delta X_8 \\ \Delta X_{11} \end{bmatrix} = \begin{bmatrix} -(X_1 + 2X_4 + X_5 + 2X_9) + d_1(X_6 + X_{10}) \\ -(X_2 + X_5 + X_6 + X_7 + 2X_8 + X_9 + 2X_{10}) - d_2(X_6 + X_{10}) \\ -(X_3 + X_7 + 2X_{11}) + d_3(X_6 + X_{10}) \\ 1 - (\sum_{i=1}^{11} X_i) - d_4(X_6 + X_{10}) \end{bmatrix}$$

Initial Value Estimation

To estimate initial values, we focus on the products generated during complete combustion. This involves narrowing the scope from the original 12 products to focus on only four key ones, specifically H_2O, CO_2, N_2, and SO_2. Additionally, we consider the products H_2, CO, O_2, and N_2, which correspond to the fractions X_4, X_6, X_8, and X_{11}, respectively. This approach establishes the following products within the combustion equation:

$$X_{13}\left({}_n C +_m H +_r O +_{r'} N +_j S\right) \Rightarrow X_4 H_2 + X_6 CO + X_8 O_2 + X_9 H_2O + CC \tag{24}$$

where $CC = X_{10}CO_2 + X_{11}N_2 + X_{12}SO_2$.

When performing the elemental balance for each constituent of the fuel in this particular case, we have $C : nX_{13} = X_6 + X_{10}, H : mX_{13} = 2X_4 + 2X_9, O : 2r_1X_{13} = X_6 + 2X_8 + X_9 + 2X_{10} + 2X_{12}, N : 2r_2X_{13} = 2X_{11}, S : jX_{13} = X_{12}$

By substituting the fractions using the constants from Section 2.2, we obtain the following:

$$X_6 = \frac{nC_{10}X_{13}}{C_{10} + \sqrt{X_8}} \tag{25}$$

$$X_4 = \frac{\frac{1}{2}mC_5X_{13}}{C_5 + \sqrt{X_8}} \tag{26}$$

$$X_{11} = r_2X_{13} \tag{27}$$

$$X_{12} = jX_{13} \tag{28}$$

$$0 = \frac{n(C_{10} + 2\sqrt{X_8})}{C_{10} + \sqrt{X_8}} + \frac{\frac{1}{2}m\sqrt{X_8}}{C_5 + \sqrt{X_8}} + \frac{2X_8}{X_{13}} + 2j - 2r_1 \tag{29}$$

The quantity of X_{13} can be accurately estimated to ensure that the sum of the molar fractions equals one.

$$X_4 + X_6 + \sum_{i=8}^{12} X_i = 1 \tag{30}$$

When the air–fuel equivalence ratio is less than or equal to 1, we can obtain a reliable estimate of X_{13} through complete combustion.

$$X_{13} = \frac{1}{\frac{m}{4} + r_1 + 2r_2} \tag{31}$$

Conversely, when the air–fuel equivalence ratio exceeds 1, a dependable estimation of X_{13} can be derived from incomplete combustion.

$$X_{13} = \frac{1}{n + \frac{m}{2} + r_2 + j} \tag{32}$$

By replacing the estimated value of X_{13} into Equation (29), we obtain X_8. Once Equation (29) is solved, the remaining unknowns can be readily determined through substitution into Equations (25)–(28). This approximation is used as the initial value for the model.

$$[X_4^{(1)}, X_6^{(1)}, X_8^{(1)}, X_{11}^{(1)}] \tag{33}$$

The previous vector approximates closely to the solution vector:

$$[X_4^{(*)}, X_6^{(*)}, X_8^{(*)}, X_{11}^{(*)}] \tag{34}$$

At each iteration, the updated vector is used to compute the partial derivatives and evaluate the functions until the two criteria of convergences (200 iterations or tolerance of 1×10^{-6}).

3. Results

3.1. Numerical Model Validation

In the research, the numerical model of the combustion process, and its validation through operating data, considered crucial parameters such as LHV, density, adiabatic flame temperature and CO emissions. The model postulates that emissions of CO_2 and other greenhouse gases are inextricably linked to ϕ. The algorithm begins with $\phi = 1$, which represents a stoichiometric mixture. It then optimizes between stoichiometric and fuel-rich mixtures ($\phi \leq 1$) with the objective of reducing emissions while maximizing energy efficiency and ensuring regulatory compliance. In the case of ideal combustion, CO_2 emissions are at their highest, while CO emissions are minimized, as illustrated in Figure 3.

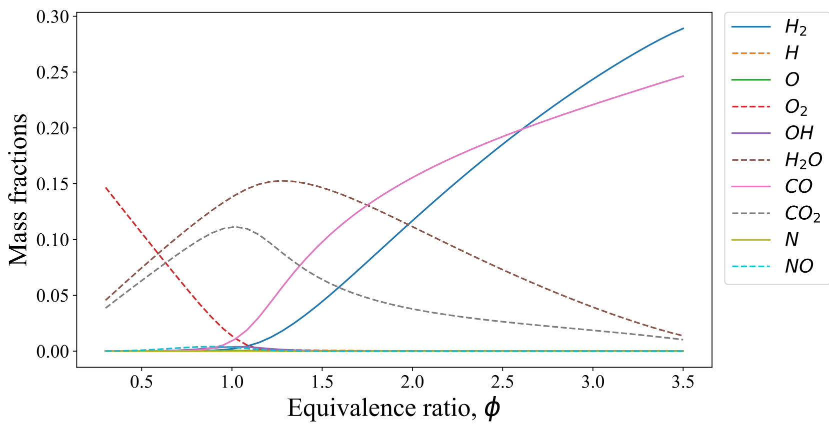

Figure 3. Levels fraction of harmful emissions.

Accordingly, the model's assumptions are constrained within a range of $\phi = 1$ to $\phi = 1.5$, where excess air is introduced to ensure more complete combustion, thereby balancing CO_2 production with lower levels of other harmful emissions, such as CO.

As shown in Figure 4, the density information for each chromatographic sample clearly shows consistent alignment between the model results (blue circles) and the data reported (red circles), thus affirming the reliability of our thermodynamic property calculations. The error is below 0.014% among the 247 samples, providing substantial validation of the computational model proposed in this research.

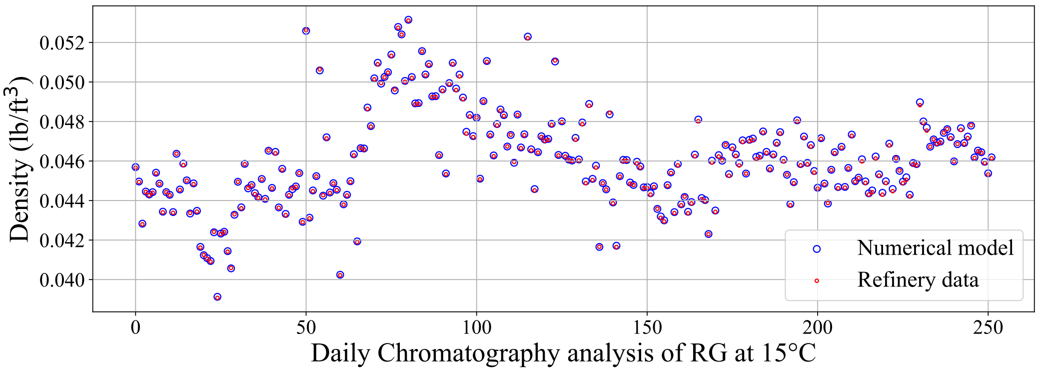

Figure 4. RG Density chromatography and model results.

On the other hand, when it comes to the computed calorific values of each specific chromatographic sample, a disparity becomes evident when compared to the reported data in Figure 5. This examination indicates that this difference can be attributed to the temperature conditions during their laboratory analysis, which plays a pivotal role. It is worth noting that each sample may exhibit a temperature falling within the range of 90 °C to 120 °C. If the exact temperatures employed for this purpose were used, this validation would likely yield results much closer to the reported values.

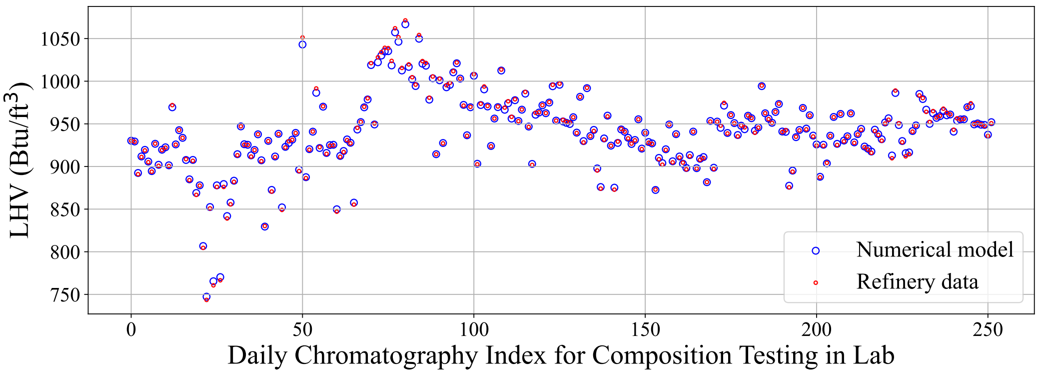

Figure 5. RG LHV chromatography and model results.

3.2. Approaches for Achieving a 50%+ Reduction in LPG Use

The algorithm for determining optimal burner flow rates is based on the principle that, regardless of the volume of crude oil processed at any given time (e.g., 100,000 barrels per day), approximately 70% of the refinery's furnace fuel demand is supplied by recovered refinery gas. This volume, in conjunction with its physicochemical properties, which are obtained through chromatographic analysis, serves as a fixed parameter at the outset of the optimization process. The objective is to achieve an LHV as close as possible to 1000 BTU/ft^3, in some cases without the need to incorporate LPG into the fuel mixture. Initially, the physicochemical characterization of gases used for combustion included determining certain properties. Table 3 presents the initial calculations of these properties such as molecular mass, density, and LHV.

NG is the usual source for the rest unless there is a significant price difference or LHV. In such cases, we introduce LPG as a third component to ensure optimal combustion [40]. Under these conditions, the numerical model of the mixing of the three gases must take into account the following considerations:

1. Calculate the mass and density of the gas mixture.
2. The LHV of the mixture must be $\geq 1000\ \mathrm{Btu/ft^3}$.
3. Obtain the adiabatic flame temperature.
4. Reducing CO_2 emissions and minimizing excess air.

Once these conditions are satisfied, the resulting mixture is optimized for combustion. Table 4 presents the blend that meets these optimization criteria.

Table 3. Physicochemical properties of gases.

Gas	Mass gmol	Density kg/m^3	Density lb/ft^3	LHV BTU/ft^3
RG_{29}	15.48	0.6558	0.04094	743.52
RG_{87}	20.06	0.8513	0.05314	1071.28
RG_{176}	17.38	0.7371	0.04601	952.62
NG	16.29	0.6907	0.04311	903.98
LPG	44.23	1.9040	0.11886	2225.47

Table 4. Properties of modeled mixtures.

Mix	*RG-NG-LPG* %-%-%	Mass gmol	Density lb/ft^3	LHV Btu/ft^3
$M_{RG_{29}}$	70-14-16	20.19	0.0537	1003.09
$M_{RG_{87}}$	70-30-00	18.92	0.0501	1021.09
$M_{RG_{176}}$	70-25-05	18.45	0.0489	1004.10

For the mixture $M_{RG_{29}}$ including the RG gas containing the lowest calorific value, the mixture simulation resulted in the following flow ratio: 70% RG, 14% NG and 16% LPG (see Table 4). It was necessary to use LPG gas due to the low calorific value contained in the refinery gas sample. In flow terms, this indicates that when the refinery gas has a calorific value greater than 1050 BTU/ft^3, it is not necessary to add LPG to the mixture. In such cases, only 70% RG and 30% NG are kept in the mixture.

As we can see in Figure 6, when applying the Newton–Raphson method to the initial values for the $M_{RG_{29}}$ mixture, the initial values converge after 70 iterations, although the blue line stops acquiring negative values and the line attempts to stabilize. Consequently, these values are replaced in the other combustion products to compute the total composition of the molecule.

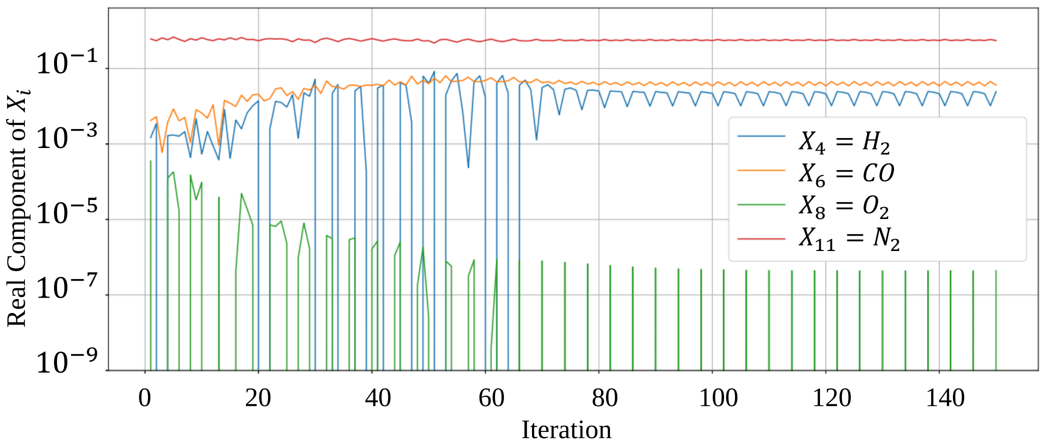

Figure 6. Newton Rhapson applied to $M_{RG_{29}}$.

The lines displayed in Figure 7 reveal that gradual changes occur after each iteration. During the initial 50 iterations, the lines extend towards the bottom of the graph in search of negative values, which is illogical as they calculate mass or volume fractions. However, they eventually stabilize, extending horizontally with a straight line after 60 iterations, indicating accurate convergence of the method. The results show that the dynamic behavior was accurate in both cases. After solving the numerical method for the three different mixture combinations and obtaining the real values of X_4, X_6, X_8, and X_{10}, these values are automatically substituted into Equations (11) to (16) to determine the exact values for the remaining combustion products. This process completes the calculation of all 12 variables. As shown in Table 5, the sum of the molar fractions confirms that they total to one, as expected.

Table 5. Combustion products, Numerical mixtures results $M_{RG_{29}}$, $M_{RG_{87}}$, $M_{RG_{176}}$.

X_i	Comb. Prod.	$M_{RG_{29}}$ MF	$M_{RG_{87}}$ MF	$M_{RG_{176}}$ MF
X_1	H	4.441×10^{-4}	3.068×10^{-4}	4.200×10^{-4}
X_2	O	1.222×10^{-6}	8.294×10^{-7}	1.090×10^{-6}
X_3	N	9.137×10^{-10}	7.540×10^{-10}	9.574×10^{-10}
X_4	H_2	4.616×10^{-2}	1.513×10^{-2}	4.019×10^{-2}
X_5	OH	1.529×10^{-4}	1.988×10^{-4}	1.238×10^{-4}
X_6	CO	5.841×10^{-2}	6.150×10^{-2}	5.742×10^{-2}
X_7	NO	2.739×10^{-5}	1.818×10^{-5}	2.461×10^{-5}
X_8	O_2	1.439×10^{-6}	3.496×10^{-7}	1.034×10^{-6}
X_9	H_2O	1.022×10^{-1}	2.133×10^{-1}	7.422×10^{-2}
X_{10}	CO_2	4.302×10^{-2}	6.817×10^{-2}	3.564×10^{-2}
X_{11}	N_2	7.496×10^{-1}	6.414×10^{-1}	7.913×10^{-1}
X_{12}	SO_2	$0.000 \times 10^{+0}$	$0.000 \times 10^{+0}$	6.621×10^{-4}
	SUM	1.00	1.00	1.00

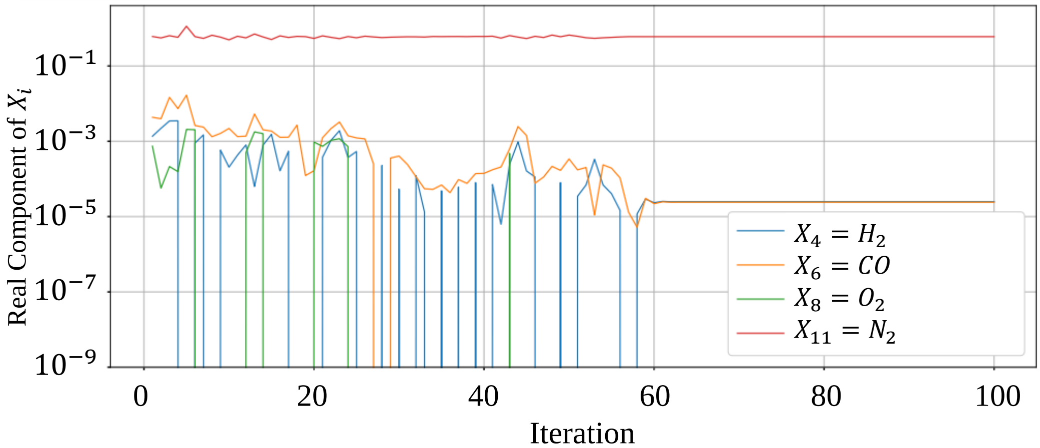

Figure 7. Newton Rhapson applied to $M_{RG_{87}}$.

4. Conclusions

This study offers a significant advance in the optimization of combustion processes in fired heaters by integrating real-time analysis of refinery gas composition. This research aims to establish a foundation for the integration of tools such as AI with immediate control in equipment that regulates the flow rates of a three-gas mixture, focusing on the variable composition of RG along with NG and LPG. This approach effectively improves combustion efficiency and reduces fuel consumption, in particular, by reducing LPG use by more than 50%, which offers significant economic benefits. The proposed improvement has the potential to reduce LPG consumption by over 50% due to the current uniform distribution of a single fuel mix (a blend of three gases) to all furnaces across the refinery, without consideration of their specific heating requirements. By customizing the fuel mix for each furnace based on its heating requirements, substantial savings are possible. For instance, furnaces in the hydrocracking unit require less energy compared to those in the primary distillation unit, which handles unrefined crude and demands higher temperatures. Tailoring the fuel supply to match these requirements improves efficiency and can lead to a reduction in LPG consumption of over 50%, particularly when NG prices are relatively higher than LPG costs

The application of GC-MS data in real-time allowed for the accurate calculation of individual compounds' mass fractions. This innovation in monitoring and adjusting the composition of the fuel mixture ensures a more consistent and efficient combustion process. The successful implementation of the Newton–Raphson method in Python to solve the non-linear equations derived from the study demonstrates the practical utility of the approach.

Furthermore, this research focus on reducing greenhouse gas emissions conforms to worldwide sustainability targets. The numerical model helps to reduce operational costs and contributes to improved efficiency and performance within petrochemical furnace systems. This research represents a noteworthy advancement in achieving more sustainable and efficient energy management within industrial processes. Additionally, it enables the storage of mass flow data on pollutant gas emissions to report these metrics in annual projections for reducing CO_2.

Author Contributions: Conceptualization, A.P.-D., R.S. and W.V.-D.; methodology, R.S., A.P.-D. and J.F.-V.; software, R.S. and W.V.-D.; validation, R.S., A.P.-D., W.V.-D. and J.F.-V.; formal analysis, W.V.-D. and J.F.-V.; investigation, A.P.-D.; resources, A.P.-D.; data curation, R.S. and A.P.-D.; writing—original draft preparation, A.P.-D., W.V.-D., R.S. and J.F.-V.; writing—review and editing, W.V.-D., A.P.-D. and J.F.-V.; visualization, R.S. and W.V.-D.; supervision, A.P.-D.; project administration, A.P.-D.; funding acquisition, A.P.-D. All authors have read and agreed to the published version of the manuscript.

Funding: The APC was funded by Universidad Tecnológica de Bolivar.

Data Availability Statement: Data are contained within the present article.

Acknowledgments: This work was supported by the Universidad Tecnológica de Bolívar under the EOLITO research group.

Conflicts of Interest: The authors declare no conflicts of interest.

References

1. Garg, A. A New Approach to Optimizing Fired Heaters. 2010. Available online: https://oaktrust.library.tamu.edu/handle/1969.1/94037 (accessed on 19 September 2024).
2. Garg, A. Optimize fired heater operations to save money. *Hydrocarb. Process.* **1997**, *76*, 97–112.
3. Litvinenko, V. The role of hydrocarbons in the global energy agenda: The focus on liquefied natural gas. *Resources* **2020**, *9*, 59. [CrossRef]
4. Filimonova, I.V.; Cherepanova, D.; Provornaya, I.; Kozhevin, V.; Nemov, V. The dependence of sustainable economic growth on the complex of factors in hydrocarbons-exporting countries. *Energy Rep.* **2020**, *6*, 68–73. [CrossRef]
5. Tcvetkov, P.; Cherepovitsyn, A.; Makhovikov, A. Economic assessment of heat and power generation from small-scale liquefied natural gas in Russia. *Energy Rep.* **2020**, *6*, 391–402. [CrossRef]
6. Garba, M.D.; Usman, M.; Khan, S.; Shehzad, F.; Galadima, A.; Ehsan, M.F.; Ghanem, A.S.; Humayun, M. CO_2 towards fuels: A review of catalytic conversion of carbon dioxide to hydrocarbons. *J. Environ. Chem. Eng.* **2021**, *9*, 104756. [CrossRef]
7. Miller, S.A.; Wilkinson, J.D.; Lynch, J.T.; Hudson, H.M.; Cuellar, K.T.; Johnke, A.F.; Lewis, W.L. Hydrocarbon Gas Processing. U.S. Patent 10,227,273, 12 March 2019.
8. Qamar, R.A.; Mushtaq, A.; Ulla, A.; Ali, Z.U. Simulation of Liquefied Petroleum Gas Recovery from Off Gases in a Fuel Oil Refinery. *J. Adv. Res. Fluid Mech. Therm. Sci.* **2020**, *73*, 109–130. [CrossRef]
9. Eshaghi, S.; Hamrang, F. An innovative techno-economic analysis for the selection of an integrated ejector system in the flare gas recovery of a refinery plant. *Energy* **2021**, *228*, 120594. [CrossRef]
10. Cala, O.M.; Stand, L.M.; Kafarov, V.; Rueda, J.S. Efecto de la composición del gas de refinería sobre las características del proceso de combustión. *Rev. Ing. Univ. Medellín* **2013**, *12*, 101–111. [CrossRef]
11. Arefin, M.A.; Nabi, M.N.; Akram, M.W.; Islam, M.T.; Chowdhury, M.W. A review on liquefied natural gas as fuels for dual fuel engines: Opportunities, challenges and responses. *Energies* **2020**, *13*, 6127. [CrossRef]
12. Amell, A.; Barraza, L.; Gómez, E. Tecnología de la Combustión de Gases y Quemadores Atmosféricos de Premezcla. Línea, Disponible. 1996. Available online: http://es.scribd.com/doc/73707395/3-Quemadores-Atmosfericos-1 (accessed on 19 September 2024).
13. Murshed, M.; Alam, R.; Ansarin, A. The environmental Kuznets curve hypothesis for Bangladesh: The importance of natural gas, liquefied petroleum gas, and hydropower consumption. *Environ. Sci. Pollut. Res.* **2021**, *28*, 17208–17227. [CrossRef]
14. Kim, S.Y.; Costa, A.L.; Bagajewicz, M.J. New robust approach for the globally optimal design of fired heaters. *Chem. Eng. Res. Des.* **2023**, *197*, 434–448. [CrossRef]
15. Ghorashi, S.A.; Khandelwal, B. Toward the ultra-clean and highly efficient biomass-fired heaters. A review. *Renew. Energy* **2023**, *205*, 631–647. [CrossRef]

16. Qasim, F.; Lee, D.H.; Won, J.; Ha, J.K.; Park, S.J. Development of Advanced Advisory System for Anomalies (AAA) to Predict and Detect the Abnormal Operation in Fired Heaters for Real Time Process Safety and Optimization. *Energies* **2021**, *14*, 7183. [CrossRef]
17. Thorat, S.; McQueen, G.; Luzunaris, P.T. The role of optimal design and application of heat tracing systems to improve the energy conservation in petrochemical facilities. *IEEE Trans. Ind. Appl.* **2013**, *50*, 163–173. [CrossRef]
18. Masoumi, M.E.; Izakmehri, Z. Improving of refinery furnaces efficiency using mathematical modeling. *Int. J. Model. Optim.* **2011**, *1*, 74. [CrossRef]
19. EU. *A Clean Planet for All, a European Long-Term Strategic Vision for a Prosperous, Modern, Competitive and Climate Neutral Economy*; Depth Analysis in Support of the Commission Communication Com; European Commission: Brussels, Belgium, 2018; Volume 773.
20. Wildy, F.; Instruments, A.P. Fired heater optimization. In *Technical Sales Support Manager*; AMETEK Process Instruments: Pittsburgh, PA, USA, 2000.
21. Rico, J.C.S.; Sánchez, Y.A.C. Análisis teórico de la combustión en quemadores de gas natural. *Sci. Tech.* **2005**, *3*, 139–143.
22. Bouras, F.; Khaldi, F. Optimization of Combustion Efficiency Using a Fuel Composition Based on CH_4 and/or H_2. *Russ. J. Appl. Chem.* **2020**, *93*, 1954–1959. [CrossRef]
23. Horbaj, P. Simulation method for optimization of a mixture of fuel gases. *Gas Waerme Int.* **2000**, *49*, 250–252.
24. Kazi, S.R.; Sundar, K.; Srinivasan, S.; Zlotnik, A. Modeling and optimization of steady flow of natural gas and hydrogen mixtures in pipeline networks. *Int. J. Hydrogen Energy* **2024**, *54*, 14–24. [CrossRef]
25. Simsek, S.; Uslu, S.; Simsek, H.; Uslu, G. Improving the combustion process by determining the optimum percentage of liquefied petroleum gas (LPG) via response surface methodology (RSM) in a spark ignition (SI) engine running on gasoline-LPG blends. *Fuel Process. Technol.* **2021**, *221*, 106947. [CrossRef]
26. Derikvand, H.; Dehaj, M.S.; Taghavifar, H. The effect of different sampling method integrated in NSGA II optimization on performance and emission of diesel/hydrogen dual-fuel CI engine. *Appl. Soft Comput.* **2022**, *128*, 109434. [CrossRef]
27. Saifullin, E.; Larionov, V.; Busarov, A.; Busarov, V. Optimization of hydrocarbon fuels combustion variable composition in thermal power plants. *J. Phys. Conf. Ser.* **2016**, *669*, 012037. [CrossRef]
28. Patrón, G.D.; Ricardez-Sandoval, L. An integrated real-time optimization, control, and estimation scheme for post-combustion CO2 capture. *Appl. Energy* **2022**, *308*, 118302. [CrossRef]
29. Cote Florez, M.S. Revision de Alternativas Operativas Para el Cumplimiento de Especificaciones de Calidad de Gas en un Campo Productor. Ph.D. Thesis, Universidad Industrial de Santander, Escuela De Ingeniería de Petróleos, Bucaramanga, Colombia, 2018.
30. Arroyo, H.; Nichiren, S.; Alonso, M.; Delfin, F. Calidad y Medición del Gas Natural. 2006. Available online: https://es.scribd.com/document/462864821/Calidad-y-medicion-del-gas-natural (accessed on 19 September 2024).
31. Chomiak, J.; Longwell, J.; Sarofim, A. Combustion of low calorific value gases; problems and prospects. *Prog. Energy Combust. Sci.* **1989**, *15*, 109–129. [CrossRef]
32. Pinzón Vargas, B.L.; Plazas Puentes, M.I. Evaluación Técnico-Financiera de las Tecnologías de Construcción Modular para la Refinación de Petróleo Crudo en el Proyecto RefiBoyacá. Bachelor's Thesis, Fundación Universidad de América, Bogotá, Colombia, 2018.
33. Qin, C.; Li, J.; Yang, C.; Ai, B.; Zhou, Y. Comparative Study of Parameter Extraction from a Solar Cell or a Photovoltaic Module by Combining Metaheuristic Algorithms with Different Simulation Current Calculation Methods. *Energies* **2024**, *17*, 2284. [CrossRef]
34. Olikara, C.; Borman, G.L. *A Computer Program for Calculating Properties of Equilibrium Combustion Products with Some Applications to IC Engines*; Technical Report; SAE Technical Paper; SAE International: Warrendale, PA, USA, 1975.
35. Lide, D.R. *CRC Handbook of Chemistry and Physics*; CRC Press: Boca Raton, FL, USA, 2004; Volume 85.
36. Turns, S.R. *Introdução à Combustão-: Conceitos e Aplicações*; AMGH Editora: Porto Alegre, Brazil, 2013.
37. Worters, M.; Millard, D.; Hunter, G.; Helling, C.; Woitke, P. Comparison Catalogue of Gas-Equilibrium Constants, Kp. 2017. Available online: https://research-repository.st-andrews.ac.uk/handle/10023/12242 (accessed on 19 September 2024).
38. Klotz, I.M. *Chemical Thermodynamics*; WA Benjamin Inc.: New York, NY, USA, 1964.
39. Yıldız, M. Chemical equilibrium based combustion model to evaluate the effects of H2 addition to biogases with different CO_2 contents. *Int. J. Hydrogen Energy* **2024**, *52*, 1334–1344. [CrossRef]
40. Way, R. Methods for determination of composition and thermodynamic properties of combustion products for internal combustion engine calculations. *Proc. Inst. Mech. Eng.* **1976**, *190*, 687–697. [CrossRef]